NEOPLASIA
www.neoplasia.com

Volume 13 Number 3 March 2011 pp. 266–275 266

Use of DNA Microarray and Small Animal Positron Emission Tomography in Preclinical Drug Evaluation of RAF265, a Novel B-Raf/VEGFR-2 Inhibitor[1,2]

Jeffrey R. Tseng*, Darrin Stuart†, Kimberly Aardalen†, Angelo Kaplan‡, Natasha Aziz§, Nicholas P. Hughes* and Sanjiv S. Gambhir*,¶

*Molecular Imaging Program at Stanford, Bio-X Program, and Department of Radiology, Stanford University, Stanford, CA, USA; †Department of Pharmacology, Novartis Institutes for Biomedical Research, Emeryville, CA, USA; ‡Department of Experimental Pathology, Novartis Institutes for Biomedical Research, Emeryville, CA, USA; §Department of Translational Biology, Novartis Institutes for Biomedical Research, Emeryville, CA, USA; ¶Department of Bioengineering, Stanford University, Stanford, CA, USA

Abstract

Positron emission tomography (PET) imaging has become a useful tool for assessing early biologic response to cancer therapy and may be particularly useful in the development of new cancer therapeutics. RAF265, a novel B-Raf/vascular endothelial growth factor receptor-2 inhibitor, was evaluated in the preclinical setting for its ability to inhibit the uptake of PET tracers in the A375M (B-Raf^{V600E}) human melanoma cell line. RAF265 inhibited 2-deoxy-2-[^{18}F]fluoro-D-glucose (FDG) accumulation in cell culture at 28 hours in a dose-dependent manner. RAF265 also inhibited FDG accumulation in tumor xenografts after 1 day of drug treatment. This decrease persisted for the remaining 2 weeks of treatment. DNA microarray analysis of treated tumor xenografts revealed significantly decreased expression of genes regulating glucose and thymidine metabolism and revealed changes in apoptotic genes, suggesting that the imaging tracers FDG, 3-deoxy-3-[^{18}F]fluorothymidine, and annexin V could serve as potential imaging biomarkers for RAF265 therapy monitoring. We concluded that RAF265 is highly efficacious in this xenograft model of human melanoma and decreases glucose metabolism as measured by DNA microarray analysis, cell culture assays, and small animal FDG PET scans as early as 1 day after treatment. Our results support the use of FDG PET in clinical trials with RAF265 to assess early tumor response. DNA microarray analysis and small animal PET studies may be used as complementary technologies in drug development. DNA microarray analysis allows for analysis of drug effects on multiple pathways linked to cancer and can suggest corresponding imaging tracers for further analysis as biomarkers of tumor response.

Neoplasia (2011) 13, 266–275

Abbreviations: CT, computed tomography; FDG, 2′-deoxy-2′-[^{18}F]fluoro-D-glucose; FLT, 3′-deoxy-3′-[^{18}F]fluorothymidine; H & E, hematoxylin and eosin; %ID/g, percent injected dose per gram; PEG, polyethylene glycol; PET, positron emission tomography; ROI, region of interest; SUV, standardized uptake value; VEGFR, vascular endothelial growth factor receptor

Address all correspondence to: Sanjiv S. Gambhir, MD, PhD; Director, Molecular Imaging Program at Stanford; Head, Division of Nuclear Medicine; Professor, Departments of Radiology and Bioengineering, Bio-X Program; The James H. Clark Center, 318 Campus Dr, East Wing, 1st Floor, Stanford, CA 94305-5427. E-mail: sgambhir@stanford.edu

[1]This work was supported in part by a research grant from Chiron Corp, now a subsidiary of Novartis (S.S.G.), and National Cancer Institute In vivo Cellular and Molecular Imaging Centers P50 CA114747 (S.S.G.).

[2]This article refers to supplementary materials, which are designated by Table W1 and Figures W1 and W2 and are available online at www.neoplasia.com.

Received 20 October 2010; Revised 6 December 2010; Accepted 8 December 2010

DOI 10.1593/neo.101466

Introduction

RAF265 is a novel, orally dosed, small-molecule B-Raf kinase and vascular endothelial growth factor receptor-2 (VEGFR-2) inhibitor with potent antitumor activity in mutant B-Raf tumor models and is currently undergoing phase 1 clinical trials in melanoma [1,2]. Inhibiting mutant B-Raf as well as VEGFR-2 provides a dual mechanism of action: antiproliferative activity by inhibiting the Ras/Raf/mitogen-activated protein kinase (MAPK) pathway and indirect antitumor activity by inhibiting angiogenesis through VEGFR-2.

2′-Deoxy-2′-[^{18}F]fluoro-D-glucose positron emission tomography (FDG PET) is a widely used clinical imaging test for many cancers and for a wide range of indications [3]. Small animal PET scanners for rodents [4] has allowed for the assessment of tumor xenograft mouse models with FDG for preclinical oncology research and drug development [5–9]. Several authors have used small animal FDG PET to assess various therapies in mouse tumor xenograft models with FDG and the proliferation tracer 3′-deoxy-3′-[^{18}F]fluorothymidine (FLT) [10–17]. We have recently shown that small animal PET studies are reproducible with moderately low variability, such that serial studies on mouse tumor xenografts are reliable in assessing therapy response [18,19].

DNA microarray analysis is a powerful technique to evaluate the expression of thousands of genes in a single experiment. Recent studies in clinical oncology have used DNA microarray analysis for identifying cancer subtypes, predicting prognosis, predicting therapy response, and understanding cancer biology [20,21]. Recently, several groups have begun to investigate the combination of FDG PET and DNA microarray analysis by correlating imaging findings with gene expression changes [22–27]. The two technologies are complementary and may provide unique insights into tumor biology. DNA microarray analysis of gene expression allows for analysis of multiple genes and multiple pathways but is limited by the need for invasive tissues sampling and may be restricted to a single time point. FDG PET is a noninvasive technology that allows for evaluation at multiple time points in the same subject without the need for invasive pathologic examination; however, it is limited to analysis of a single pathway, namely glucose metabolism albeit a very useful one for most cancers.

In this study, our first objective was to use DNA microarray analysis to suggest pathways affected by RAF265, which have corresponding imaging agents that could potentially serve as imaging biomarkers. Our second objective was to assess whether small animal FDG PET could be used to assess the efficacy of RAF265 in the A375M (B-Raf^{V600E}) mouse xenograft tumor model. We show that RAF265 inhibited the glucose metabolism pathway and was confirmed by inhibition of FDG accumulation both in cell culture and in tumor xenografts.

Materials and Methods

Pharmaceutical

RAF265 (Novartis, Emeryville, CA) is a novel, orally bioavailable, small-molecule inhibitor of Raf kinase/VEGFR-2 with a molecular weight of 518 g/mol. For cell culture experiments, the drug was dissolved in dimethyl sulfoxide. For *in vivo* mouse xenograft experiments, the drug was dissolved in polyethylene glycol-400 (PEG-400) to a concentration of 25 mg/ml.

Cell Culture

A375M human melanoma cells, which express B-Raf^{V600E}, were grown in minimum essential medium with Earle salts and L-glutamine, supplemented with 10% fetal bovine serum, 1 mM sodium pyruvate, and 1× nonessential amino acids (Mediatech, Manassas, VA). MV4;11 human acute myelogenous leukemia cells, which express wild-type B-Raf, were grown in Iscove modified Dulbecco medium with L-glutamine and 25 mM HEPES, supplemented with 10% fetal bovine serum and 5 ng/ml granulocyte macrophage colony-stimulating factor. Cells were grown at 37°C with 5% CO_2 in a humidified incubator. For xenograft implantation, cells were resuspended in Hank's balanced salt solution (Mediatech).

Cell Culture FDG, FLT, and Proliferation Assays

Fifty thousand A375M or MV4;11 cells were plated overnight onto 24-well plates. After changing the medium, 1.0 μM RAF265, 0.1 μM RAF265, or no drug (solvent control) was added to the wells in triplicate and incubated for 4 to 5 hours and 24 to 28 hours. Approximately 1 μCi of FDG (PETNET or Stanford Radiochemistry Facility) was added and incubated for 2 hours. Cells were rinsed with cold phosphate-buffered saline (Invitrogen, Carlsbad, CA) and then lysed with 1 N NaOH. Half of the sample was counted for radioactivity using a Cobra II gamma counter (Packard, Meriden, CT). The remaining sample was used to determine protein concentration with a Bradford protein assay (Bio-Rad, Hercules, CA). FDG accumulation was calculated as: FDG accumulation (%/mg) = FDG activity within the cells (cpm) ÷ total FDG added to the sample (cpm) ÷ total protein (mg) × 100%. FLT assays for A375M cells were performed in a similar manner using a 1-hour incubation period for FLT accumulation. FLT was synthesized by the Stanford Radiochemistry Facility with a specific activity greater than 45 TBq/mmol [18]. Proliferation assays on cell lines were performed by incubating cells with RAF265 diluted in complete medium over a concentration range of 0.1 to 20 μM in 96-well plates. After 72 hours of incubation, cells were rinsed, and then the CellTiter-Glo assay was carried out as described by the manufacturer (Promega, Madison, WI).

Mouse Xenograft Model for Tumor DNA Microarray Analysis

Animal protocols were approved by the Stanford Administrative Panel on Laboratory Animal Care and the Novartis Institutional Animal Care and Use Committee. Forty-five 8-week-old *nu/nu* mice (Charles River Laboratory) were injected subcutaneously with 3 million A375M cells in the right flank. After approximately 1 week when xenografts reached a size of approximately 200 mm^3, five mice were killed immediately as baseline controls (day 0). Tumors were harvested and frozen. The remaining mice were separated into groups of five. Half of the groups were orally dosed with 100 mg/kg of RAF265 (approximate volume of 100 μl) every 2 days for 14 days. The other half were orally dosed with vehicle PEG-400. Mice were killed, and tumors were harvested at 8 hours, day 1, day 8, and day 14.

RNA was extracted from the tumor xenografts using an RNeasy kit (Qiagen). Complementary DNA and RNA were synthesized. Complementary RNA was labeled and hybridized to a human genome U133 Plus 2.0 microarray (Affymetrix, Santa Clara, CA). Data were normalized using the MAS 5.0 software (Affymetrix).

The Gene Set Enrichment Analysis (GSEA) method [28,29] was used to identify coordinate changes in biologic pathways modulated by RAF265. The effects of RAF265 *versus* vehicle at each of the four time points were mapped to 4014 publicly available pathways (KEGG [Kanehisa Laboratories, Kyoto, Japan; n = 361 pathways], Panther [SRI International, Palo Alto, CA; n = 1698 pathways], and Metacore pathways [GeneGo, St Joseph, MI; n = 1955]) using an in-house

implementation of GSEA as previously described [30]. A subset of those results including pathways with corresponding molecular tracers available is presented. Thirty-four major reference pathways for apoptosis (apoptosis/annexin V) or containing glucose transporters and/or hexokinases (Entrez Gene IDs 6513, 6514, 6515, 6517, 6518, 11182, 155184, 29988, 56606, 81031, 66035, 154091, 114134, 144195, 3098, 3099, 3101, 2645), thymidine kinase (Gene ID 7083), and epidermal growth factor receptor (EGFR; Gene ID 1956) were identified (Table W1). Pathways considered significantly modulated by RAF265 had a q value (reflecting the false discovery rate) $\leq 1 \times 10^{-5}$ [31].

Mouse Xenograft Model for Small Animal FDG PET

A separate group of forty 8-week-old female *nu/nu* mice was injected subcutaneously with 3 million A375M cells in the right upper flank. When tumors reached an approximate volume of 100 mm^3, eight mice were selected for cohort 1 ($n = 4$ control; $n = 4$ drug-treated group). When tumors reached an approximate volume of 200 mm^3, 12 mice were selected for cohort 2 ($n = 6$ control; $n = 6$ drug-treated group). Mice were weighed, and tumors were measured with digital calipers every 2 to 3 days. Tumors volumes were calculated using orthogonal measurements as length × width × width ÷ 2.

The drug dosing and imaging schedules were as follows. Mice were administered 100 mg/kg RAF265 or vehicle (100% PEG-400) by oral gavage every 3 days starting on day 0 and continuing to day 15. For cohort 1 (starting tumor volume = 100 mm^3), a day 0 baseline small animal FDG PET scan was performed immediately before the first drug dose, followed by imaging on days 1, 4, 7, 11, and 13. For cohort 2 (starting tumor volume = 200 mm^3), mice were imaged on days 0, 1, 4, 7, 9, 10 or 11, 14, and 16. On day 9, imaging was performed before dosing. Owing to the limited availability of tracer, only four mice were scanned on days 9, 14, and 16 for the control group of cohort 2. Data for day 10 or 11 were combined and analyzed together using a middle time point of 10.5 days. One mouse in the drug-treated group of cohort 2 died during scanning on Day 11, thereafter only three mice were scanned on days 14 and 16 for the drug-treated group of cohort 2. The mouse that died had no overt signs of toxicity, such as illness, distress, or significant weight loss. In our experience, a death rate of approximately 1% during scanning is expected, which may be related to anesthesia, tumor burden, repeated tail injections, or a combination of these factors. The single mouse death was most likely related to scanning factors rather than drug toxicity. No body weight loss or other toxicity was observed in the remaining mice.

Small Animal FDG PET Imaging

Imaging was performed as previously described and summarized below [18,19]. After a 4- to 6-hour fast, approximately 200 μCi of FDG was injected through the tail vein. One hour after injection, a 7-minute static prone scan was obtained in a MicroPET R4 (Siemens/CTI, Munich, Germany) without partial volume correction [32]. A sample three-dimensional rendering of a tumor-bearing mouse is included as Figure W1.

Small Animal FDG PET Image Analysis

Ellipsoidal regions of interest (ROIs) were drawn around the edge of the tumor activity using AMIDE software [33]. The mean, the mean of the upper 20% of voxels, and the maximum activities were recorded. Percent injected dose per gram (%ID/g) and standardized uptake value (SUV) were calculated as follows: %ID/g = ROI activity ÷ injected dose. SUV = ROI activity ÷ injected dose × body weight. Two separate 5-mm background ROIs were drawn from the muscle adjacent to the tumor and in the opposite flank. Tumor-to-background ratios were calculated.

Immunohistochemistry

Immunohistochemistry staining was performed on a separate set of tumors treated with a similar drug regimen. Hematoxylin and eosin (H & E) staining was performed to assess areas of viable tissue and necrosis. Ki-67 staining was performed to assess areas of proliferation.

Statistical Analysis

For cell culture and small animal FDG PET studies, t tests were performed to assess for significant differences between two groups of data. For a comparison among three groups of data, analysis of variance was first performed. If the analysis of variance was significant, pairwise comparisons were then performed. $P < .05$ was chosen to indicate significance. Data were reported with SEM error bars or error values.

Results

RAF265 Inhibits Glucose and Thymidine Metabolism Gene Expression as Determined by DNA Microarray Analysis

A pathway-based analysis of gene expression in A375M xenografts from mice treated with RAF265 showed that RAF265 had profound inhibitory effects on the cell cycle at all time points examined (data not shown). Consistent with this, glucose metabolism, thymidine metabolism, and apoptosis pathways were modulated by RAF265 (Table 1 and Figure 1). A summary diagram of effects of RAF265 on the glucose metabolism pathway is provided in Figure W2. EGFR pathways were not transcriptionally modulated by RAF265 (Table W1). This suggested that FDG (glucose metabolism), FLT (thymidine metabolism), and annexin V (apoptosis) tracers may be useful in RAF265 imaging studies.

RAF265 Inhibits FDG Accumulation in A375M Cell Culture

A375M cells were incubated with two different concentrations of RAF265 for 5 and 28 hours then assayed for FDG accumulation. At 28 hours, RAF265 treatment resulted in a significant dose-dependent inhibition of FDG accumulation compared with controls (untreated cells; Figure 2*A*). At 1.0 μM, RAF265 had a more significant decline in FDG accumulation (75.5%, $P = .0003$) compared with the lower concentration of 0.1 μM (38.2%, $P = .02$) compared with control. At the earlier 5-hour time point, RAF265 did not show significant inhibition. These results are consistent with potent antiproliferative activity of RAF265 in these cells ($IC_{50} = 0.28$ μM).

To determine whether the effect of RAF265 was selective for cells expressing mutant B-Raf, FDG accumulation was also evaluated in the human acute monocytic leukemia cell line MV4;11, which expresses wild-type B-Raf. At 4 and 24 hours, FDG accumulation in drug-treated MV4;11 cells was not significantly different from control at both 1.0 and 0.1 μM (Figure 2*B*). These results were consistent with the lack of antiproliferative activity of RAF265 on these cells ($IC_{50} = 6$ μM).

Table 1. Pathways Modulated by RAF265 in A375M Xenografts.

Time Point	Rank	Pathway	Pathway Data Source	Pathway ID	Pathway Name	No. Probe Sets	*P*	*q*
Day 1: 8 h	32	Thymidine	KEGG Pathways	map00240	Pyrimidine metabolism — Reference pathway	83	1.17*e* – 12	8.07*e* – 11
Day 1: 8 h	69	Glucose	MetaCore Pathway Maps	S8	Carbohydrates metabolism	264	3.11*e* – 08	1.09*e* – 06
Day 1: 8 h	75	Thymidine	MetaCore Pathway Maps	S11	Nucleotide metabolism	224	2.45*e* – 07	7.46*e* – 06
Day 1: 24 h	45	Glucose	MetaCore Pathway Maps	S8	Carbohydrates metabolism	264	5.05*e* – 09	2.07*e* – 07
Day 1: 24 h	61	Thymidine	KEGG Pathways	map00240	Pyrimidine metabolism — Reference pathway	83	2.69*e* – 08	8.38*e* – 07
Day 1: 24 h	76	Apoptosis	MetaCore Pathway Maps	S121	Apoptosis and survival	242	1.20*e* – 07	3.10*e* – 06
Day 8	35	Thymidine	KEGG Pathways	map00240	Pyrimidine metabolism — Reference pathway	83	7.11*e* – 15	3.74*e* – 13
Day 8	66	Thymidine	MetaCore Pathway Maps	S11	Nucleotide metabolism	224	4.15*e* – 11	1.25*e* – 09
Day 8	122	Glucose	MetaCore Pathway Maps	930	Glycolysis and gluconeogenesis (short map)	33	8.63*e* – 08	1.40*e* – 06
Day 8	132	Glucose	MetaCore Pathway Maps	S8	Carbohydrates metabolism	264	2.14*e* – 07	3.23*e* – 06
Day 8	141	Apoptosis	MetaCore GeneGo Processes	131161	Apoptosis_Apoptotic mitochondria	85	3.44*e* – 07	4.88*e* – 06
Day 14	33	Thymidine	KEGG Pathways	map00240	Pyrimidine metabolism — Reference pathway	83	8.88*e* – 16	4.29*e* – 14
Day 14	65	Thymidine	MetaCore Pathway Maps	S11	Nucleotide metabolism	224	1.82*e* – 12	5.28*e* – 11
Day 14	96	Apoptosis	MetaCore Pathway Maps	S121	Apoptosis and survival	242	4.95*e* – 10	9.88*e* – 09
Day 14	133	Glucose	PANTHER Library and Pathways	MF00109	Carbohydrate kinase	26	2.73*e* – 08	3.95*e* – 07
Day 14	151	Apoptosis	MetaCore GeneGo Processes	131161	Apoptosis_Apoptotic mitochondria	85	6.23*e* – 08	8.02*e* – 07
Day 14	156	Glucose	MetaCore Pathway Maps	S8	Carbohydrates metabolism	264	7.28*e* – 08	9.07*e* – 07
Day 14	163	Glucose	MetaCore Pathway Maps	930	Glycolysis and gluconeogenesis (short map)	33	1.31*e* – 07	1.55*e* – 06

Reference pathways modulated by RAF265 ($q \leq 1 \times 10^{-5}$) and containing genes relevant to FDG (glucose), FLT (thymidine), annexin V (apoptosis), and EGFR tracer modalities are indicated. Time of RAF265 or vehicle control treatment (Time Point), the rank (by *q* value) of pathway within a time point (4014 pathways evaluated per time point), source of gene pathway (Pathway Data Source), pathway reference number (Pathway ID), name for the pathway used by the Pathway Data Source (Pathway Name), number of probe sets analyzed for each pathway (No. Probe Sets), *P* value, and *q* value are indicated. GSEA results are in Table W1.

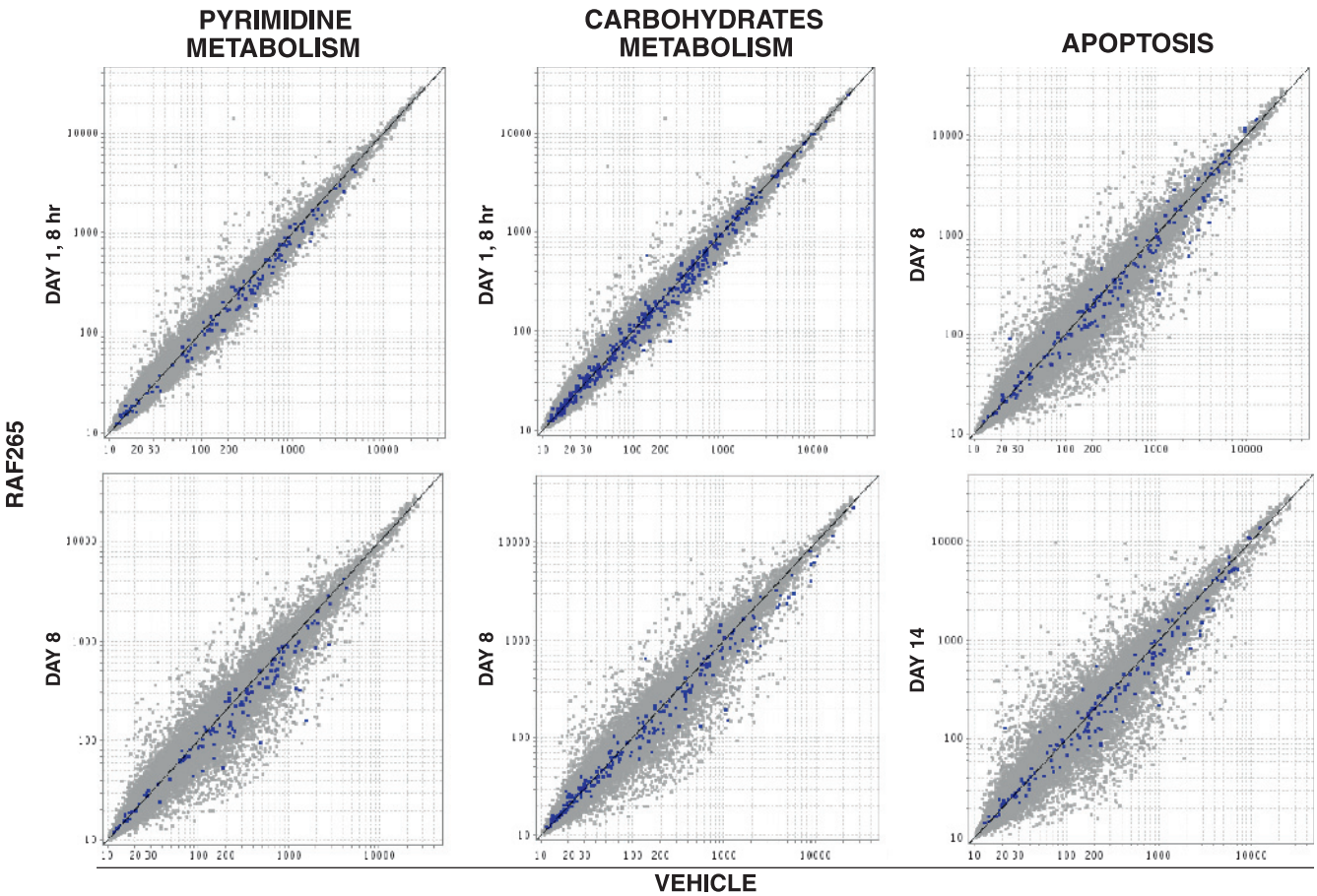

Figure 1. Scatter plot representation of pathways modulated by RAF265 in A375M xenografts. The effects of RAF265 (*y*-axis in each scatter plot) *versus* vehicle (*x*-axis) on selected individual biologic pathways from Table 1 (pyrimidine metabolism [Pathway ID map00240], carbohydrates metabolism [Pathway ID S8], apoptosis [Pathway ID 131161]) significantly modulated by RAF265 are shown at selected time points. The relative expression of all probe sets (gray dots) and gene set–specific probe sets (blue dots) are indicated (log-log scale).

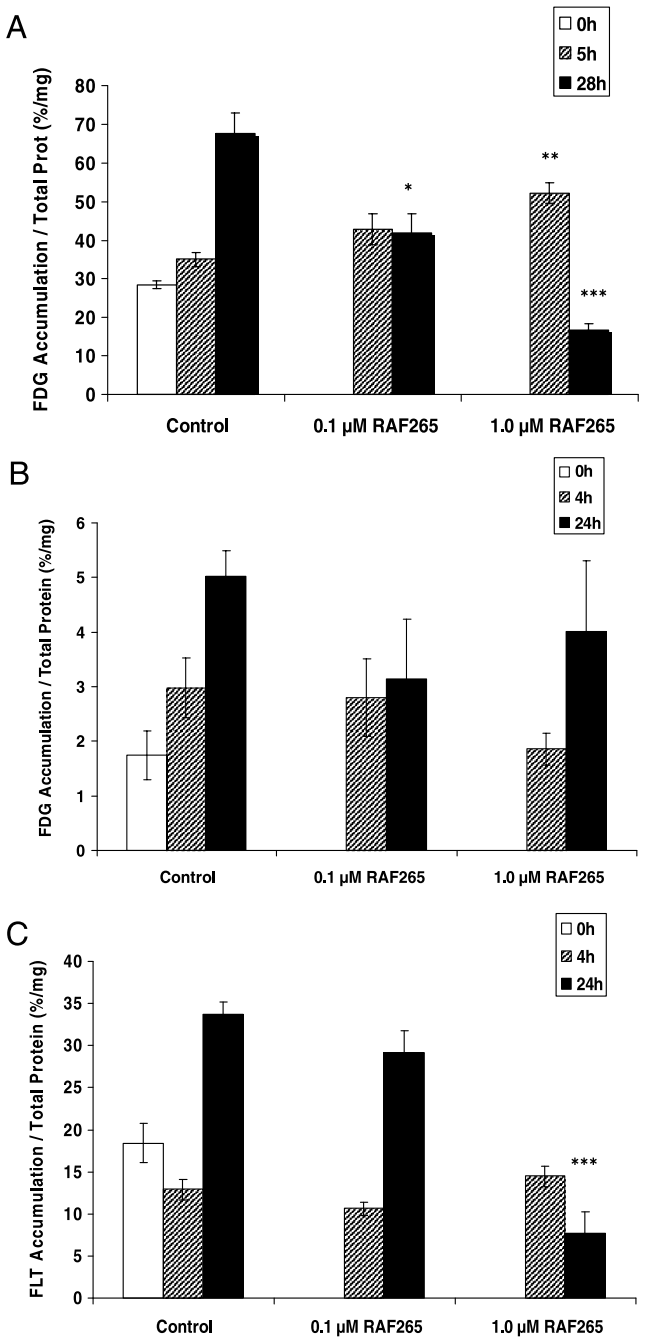

Figure 2. Cell cultures were treated with two concentrations of RAF265 drug for 5 and 28 hours and then assayed for FDG accumulation. (A) FDG accumulation in A375M cells was inhibited by RAF265 in a dose-dependent manner at 28 hours (black bars). (B) There was no significant inhibition of FDG accumulation by RAF265 in MV4;11 cells. (C) A375M cells were treated with two concentrations of RAF265 drug for 4 and 24 hours and then assayed for FLT accumulation. RAF265 inhibited FLT accumulation at 24 hours with the 1.0 μM RAF265 concentration. Error bars represent SEM. *P* values according to *t* test for comparisons between RAF265 and controls are indicated (*$P < .05$, **$P < .01$, and ***$P < .001$).

RAF265 Inhibits FLT Accumulation in A375M Cell Culture

The DNA microarray data indicating inhibition of thymidine kinase containing pathways by RAF265 suggested that RAF265 should also inhibit the uptake of FLT. Therefore, A375M cells were incubated with two different concentrations of RAF265 for 4 and 24 hours then assayed for FLT accumulation. At the earlier 4-hour time point, RAF265 did not significantly inhibit the uptake of FLT; however, by 24 hours, there was a significant decrease in FLT accumulation at 1.0 μM ($P < .0001$) but not at 0.1 μM ($P = .24$; Figure 2*C*). Because FLT inhibition was only significant at the higher dose of RAF265 and only at 24 hours compared with FDG, it was concluded that FDG may be a slightly more sensitive tracer as an imaging biomarker to test in an *in vivo* tumor xenograft model. No further testing was performed with FLT.

RAF265 Inhibits FDG Accumulation in A375M Xenografts

Nude mice with A375M tumor xenografts were dosed orally with 100 mg/kg RAF265 every 3 days at two different starting tumor volumes of 100 mm^3 for cohort 1 and 200 mm^3 for cohort 2 (Figure 3*A*). Tumor volumes for the control mice increased two- to three-fold during the study, whereas the tumor volumes decreased 51.0% and 35.1% for drug-treated cohorts 1 and 2, respectively.

FDG accumulation was assessed during 2 weeks in the same mice. Representative small animal FDG PET images for a RAF265-treated mouse (Figure 4*A*) and a control mouse (Figure 4*B*) revealed inhibition of FDG accumulation by RAF265. For the RAF265-treated mice in cohort 1 (Figure 3*B*), the mean %ID/g of FDG accumulation decreased 28.2% on day 1 compared with the baseline day 0 and showed a statistically significant difference compared with the cohort 1 control group ($P = .0001$). The FDG accumulation continued to decrease for the drug-treated group, reaching a maximum decrease of 51.0% at day 13. The drug-treated group remained significantly decreased from the control group at all time points after day 0.

For cohort 2, the mean %ID/g of FDG accumulation decreased in the drug-treated group on day 1 by 30.9% compared with the baseline day 0 (Figure 3*B*). FDG accumulation was significantly lower in the drug-treated group than the control group on day 1 ($P = .04$) and day 4 ($P < .0001$). After day 7, FDG accumulation was lower in the control group compared with the RAF265-treated group. Visual inspection of the images revealed central photopenia, suggestive of tumor necrosis, in tumors greater than approximately 300 mm^3. As the tumors increased in size, the central photopenia also increased (Figure 4*C*). Visual inspection of excised tumors suggested central necrosis in the larger tumors. This observation may partly explain the decrease in the mean %ID/g over time for the control tumors. To confirm, tissue sections of a representative tumor from a mouse under a similar dosing schedule also showed tumor necrosis with H & E staining and corresponding areas of decreased proliferation with Ki-67 staining (Figure 5).

Analysis of the max %ID/g, upper 20% %ID/g, SUV, and tumor-to-background ratios produced similar results and statistical significance to the mean %ID/g analysis (data not shown). Analysis of data normalized to the baseline day 0 was also similar.

Comparison of FDG Accumulation versus Tumor Volume

To assess the early response to RAF265, day 1 data were further analyzed. Compared with baseline, FDG accumulation decreased 28.2% and 30.9% for cohorts 1 and 2, whereas tumor volumes decreased only 14.9% and 5.2%, respectively (Figure 3*C*). In cohort 1, both FDG accumulation ($P = .0001$) and tumor volume ($P = .01$) were significantly different compared with controls; however, in cohort 2, only FDG decreased significantly compared with control ($P = .04$), whereas the decrease in tumor volume was not significant

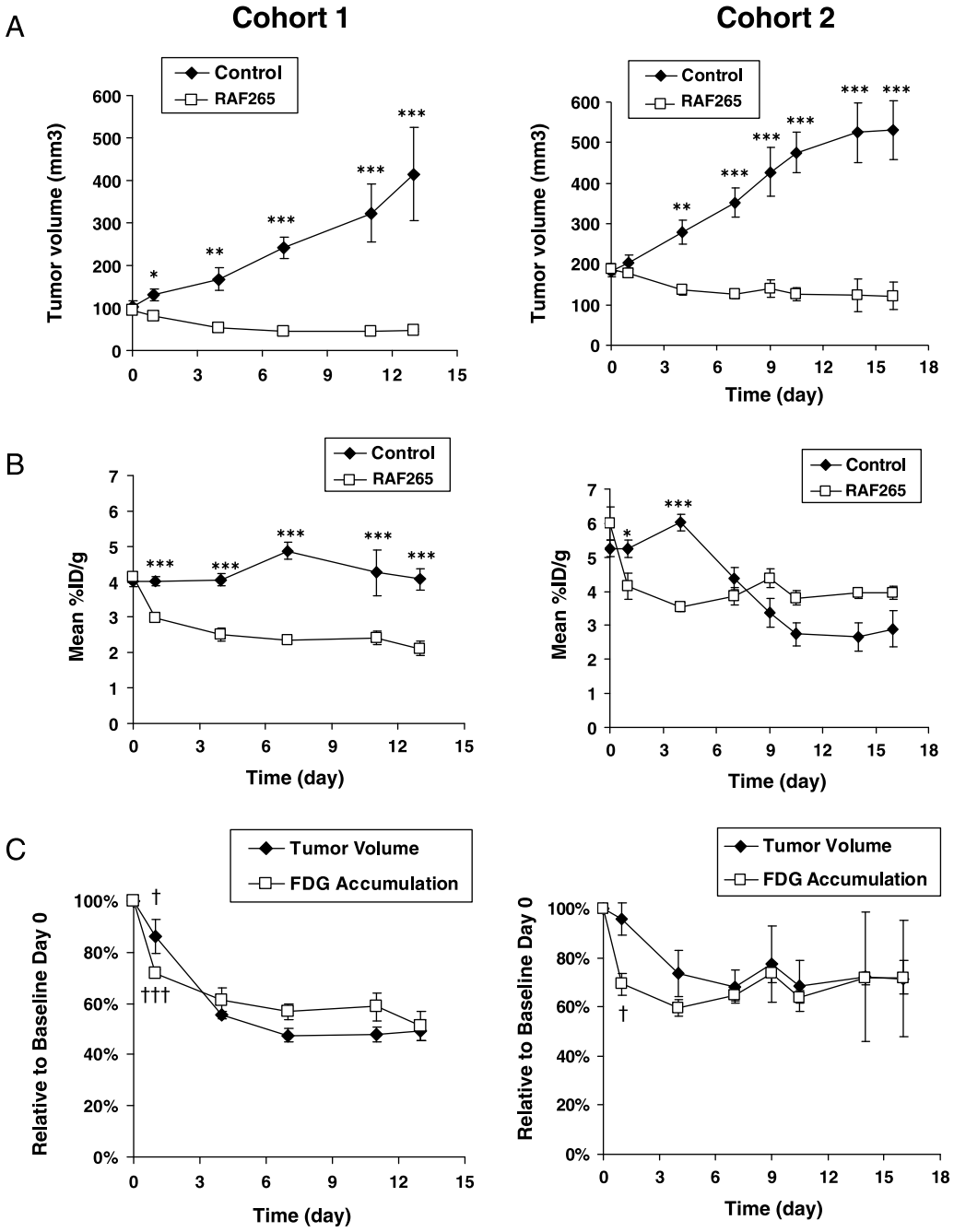

Figure 3. (A) Tumor volume growth curves for A375M xenografts treated with 100 mg/kg RAF265 or PEG-400 (control) dosed every 3 days. Cohort 1 (left) had a starting tumor volume size of 100 mm^3 ($n = 4$). Cohort 2 (right) had a starting tumor volume size of 200 mm^3 ($n = 6$). Error bars represent SEM. *P* values according to *t* test for comparisons between RAF265 and vehicle control are indicated (*$P < .05$, **$P < .01$, and ***$P < .001$). (B) Mean %ID/g FDG accumulation assayed with small animal FDG PET. Cohort 1 (left) and cohort 2 (right) showed a significant decrease in FDG accumulation for the RAF265 drug-treated groups compared with the control groups as early as day 1. (C) Comparison of tumor volume and FDG accumulation curves for the RAF265-treated A375M xenografts. Values are shown as a percentage of the baseline day 0 value. The FDG accumulation curves indicate that there is a significantly greater fold reduction at day 1 compared with the tumor volume for both cohorts. *P* values for comparisons relative to baseline day 0 are indicated ($^{\dagger}P < .05$ and $^{\dagger\dagger\dagger}P < .001$).

($P = .25$). This analysis supports the hypothesis that FDG accumulation is an earlier, more sensitive measure of antitumor activity.

Discussion

In this study, our first objective was to use DNA microarray analysis to select appropriate tracers for PET imaging. We assessed whether changes in expression of genes involved in glucose metabolism, thymidine metabolism, apoptosis, or EGFR signaling could provide insight into which PET tracers might be effective in melanoma by performing a pathway-based analysis on DNA microarray data from RAF265-treated A375M xenografts. RAF265 significantly modulated glucose metabolism, pyrimidine metabolism, and apoptosis pathways,

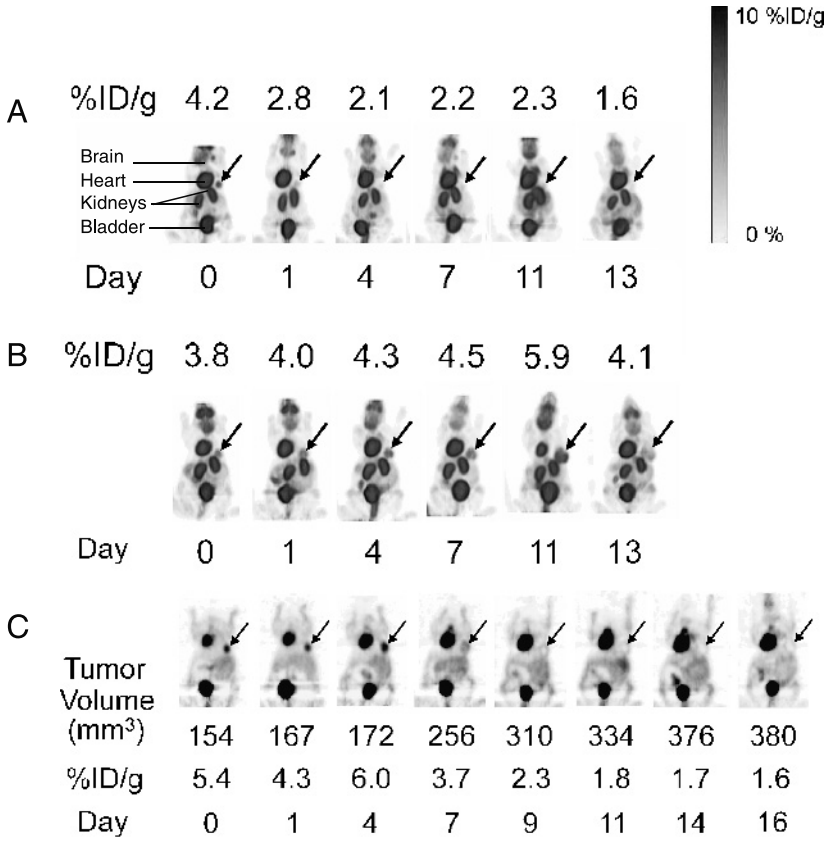

Figure 4. Three-dimensional volume renderings of small animal FDG PET images of nude mice bearing A375M xenografts (arrows). (A) Cohort 1 drug-treated tumor from baseline day 0 to day 13 of treatment with 100 mg/kg RAF265. By day 13, the activity had dramatically decreased. (B) Cohort 1 control tumor from baseline day 0 to day 13 of treatment with vehicle (PEG-400). FDG accumulation gradually increased over time. (C) Coronal small animal FDG PET images of an A375M mouse tumor xenograft from the control group of cohort 2 reveal the internal characteristics of the tumor. Images are displayed during 16 days with tumor sizes and mean %ID/g FDG accumulation listed below. The tumor (arrows) showed increasing central necrosis for tumor sizes greater than 300 mm^3.

suggesting that FDG, FLT, and annexin V, but not EGFR-based imaging modalities, may have utility. The modulation of glucose metabolism was consistent with the subsequent results, demonstrating that FDG accumulation was inhibited in cell culture and in the mouse tumor xenograft model.

It will be interesting to examine cell accumulation and small animal PET imaging for all four tracers in both cell lines and animal studies. We plan to perform a larger study where several tracers are investigated in several drug-resistant and drug-sensitive cell lines and xenografts to establish a more comprehensive relationship between tracer efficacy and changes in gene expression. It may be possible to correlate tracer efficacy to gene expression changes using a much smaller cohort of genes representing imaging-relevant biologic pathways. In this case, the resource-intensive DNA microarray approach could be substituted with interrogation of a panel of key genes by quantitative polymerase chain reaction. Because RAF265 inhibits VEGF-induced angiogenesis [34] as well as mutant B-Raf, angiogenesis pathways and new emerging tracers for imaging angiogenesis will also be investigated to assess the relative strengths of the dual mechanism of action.

Our second objective was to determine whether FDG PET could be used to assess the efficacy of RAF265. We first demonstrated that RAF265 inhibited FDG accumulation in A375M human melanoma cell culture in a dose-dependent manner (Figure 2*A*). We subsequently demonstrated that RAF265 inhibited FDG accumulation in an A375M mouse tumor xenograft model as early as 1 day of drug treatment (Figure 3, *B* and *C*) using small animal FDG PET. Significant effects of RAF265 of FDG accumulation were observed before tumor volume changes and persisted during the entire 2 weeks of the experiment. Furthermore, significant inhibition of FDG accumulation was consistent with down-regulation of the genes involved in the uptake and trapping of FDG, as assessed by gene expression analysis.

RAF265 is currently in phase 1 clinical trials for melanoma, and we anticipate that clinical FDG PET will play a central role in assessing early response to treatment based on these preclinical results. We are unaware of any published studies that have used small animal FDG PET followed by validation with clinical FDG PET. This study may serve as a model for how PET and molecular imaging can improve the drug development process by validating imaging modalities before initiation of phase 1 trials. Follow-up analysis will be performed after the conclusion of phase 1 trials to determine the predictive value of these preclinical studies.

Although few studies that used FDG PET for monitoring therapeutic response in clinical trials exist in the literature, we believe that PET can and should be used to assess response to therapy based on its proven utility in clinical practice [35]. FDG PET may serve as an exemplary marker in clinical trials of novel melanoma drugs based on the ability of PET to follow therapy response in other tumors [36] and based on the excellent ability of FDG PET to detect melanoma

[37]. As an example, a small phase 2 trial of a novel polyamine synthesis inhibitor showed that FDG PET was an early predictor of a poor response in metastatic melanoma [38]. In addition, a recent phase 1 dose-escalation trial of a mutant BRAF inhibitor showed markedly decreased tumor FDG uptake at day 15 of treatment of metastatic melanoma [39]. FDG PET could be invaluable in the clinical development of novel targeted agents such as RAF265. The current paradigm in dose determination for these agents is based more on the optimal biologic dose rather than the traditional maximal tolerated dose [40]. A noninvasive method such as FDG PET could be an excellent tool to determine the optimal biologic dose and to assess tumor response for RAF265 in melanoma patients.

FDG PET has an advantage over anatomic imaging in that changes in FDG accumulation can often be seen earlier than change in anatomic size. In our study, we observed that changes in FDG accumulation were larger and observed earlier compared with tumor volume changes. These changes occurred on the time scale of days in the mouse model, which may translate to a time scale of weeks for patients or possibly sooner. The ability of FDG PET to see earlier changes may significantly impact treatment decisions and survival. Our preclinical imaging results are in agreement with previous work from our group [13], others [17], and in clinical studies [41].

On the basis of these results, we propose a stepwise approach to select a suitable imaging tracer for tumor evaluation. Gene expression analysis is first performed on tumor cells treated with drug *in vitro* to interrogate molecular pathways that have corresponding imaging tracers. Pathways that are most affected will suggest which imaging tracers can be used in subsequent tracer accumulation studies in cell culture and small animal PET studies in mouse xenograft models.

In human clinical studies, the choice of an imaging biomarker for cancer is limited to a few modalities. Most oncology studies are performed with contrast enhanced computed tomography (CT) and/or FDG PET/CT, with a few other imaging modalities for more specialized applications, such as contrast-enhanced magnetic resonance imaging (MRI) for brain and musculoskeletal tumors, somatostatin receptor imaging for neuroendocrine tumors, iodine 123 (^{123}I) for thyroid cancer, and [^{123}I]metaiodobenzylguanidine for pheochromocytoma. Many new imaging modalities and agents are in development, such as whole-body diffusion-weighted MRI, [^{18}F]fluoromisonidazole PET for tumor hypoxia, and VEGFR imaging for angiogenesis [42–44]. With the increasing availability of molecular imaging agents, the selection of the most optimal tracer may be more challenging in the future. Gene expression profiling has the potential to assist with the selection of an appropriate imaging agent. To be useful, gene expression analysis of changes in gene expression must be correlated with imaging agent features. One revealing example was provided by the study of Segal et al. [45], where CT imaging traits of liver tumors were correlated with gene expression profiles. Other works have also been performed to correlate gene expression profiles with FDG PET [22–27]. In the future, tailored or personalized imaging biomarkers through rational selection may become more prevalent, much like personalized therapies have been envisioned.

This article attempts to unite DNA microarray and small animal PET analysis within the context of drug development and therapy evaluation. The studies presented here provide a model for translational research using DNA microarray technology, cell culture assays, and *in vivo* small animal PET studies, which can direct the selection of an appropriate PET tracer for human clinical studies.

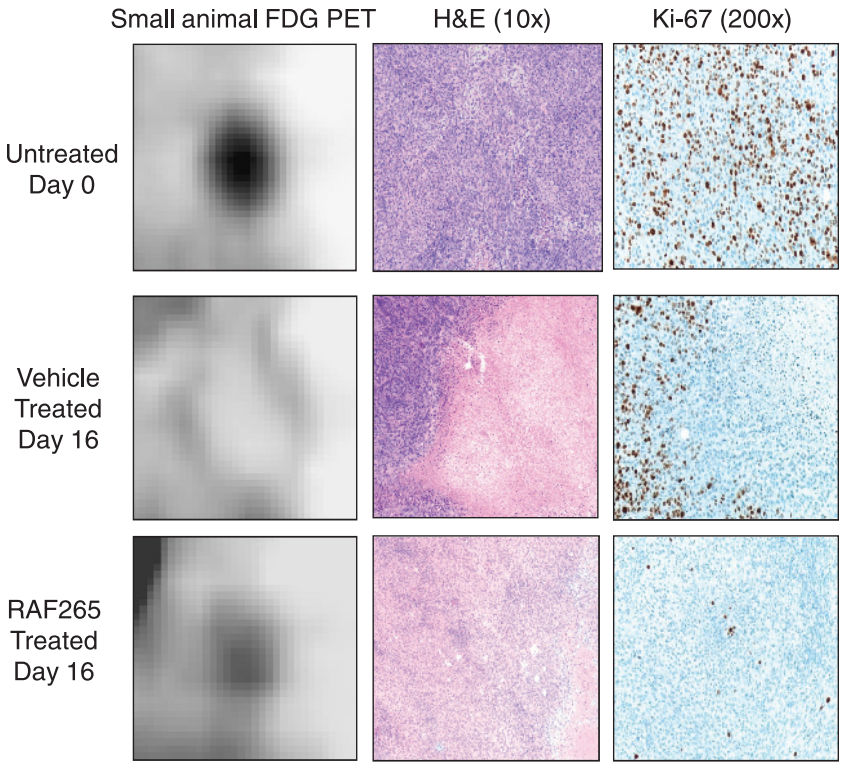

Figure 5. Magnified coronal small animal FDG PET images of vehicle-treated and RAF265-treated A375M tumor xenografts. Pathologic staining with H & E shows areas of nonviable tumor and tumor necrosis. Pathologic staining with Ki-67 shows corresponding areas or absence of tumor proliferation.

Conclusions

We would like to offer one specific conclusion regarding RAF265 and two general conclusions regarding DNA microarray analysis and small animal PET. 1) RAF265 is an efficacious novel B-Raf/VEGFR-2 inhibitor, which causes decreases in tumor glucose metabolism and FDG accumulation as early as 1 day after treatment in our preclinical model. The small animal FDG PET results support the decision to proceed with clinical trials and also support the use of human clinical FDG PET to assess early tumor response in ongoing phase 1 trials of RAF265 for melanoma. 2) DNA microarray analysis and small animal PET are complementary technologies that can each serve as a biomarker to assess glucose metabolism within the context of drug development for drug evaluation. 3) DNA microarray analysis can screen multiple pathways involved in cancer. Significant changes can be used to select corresponding molecular imaging agents for further cell culture and *in vivo* evaluation.

Acknowledgments

The authors thank Andreas Loening for assistance with image analysis, Shay Karen at the Stanford Small Animal Imaging Facility for assistance with small animal PET imaging, and Frederick Chin and David Dick at the Stanford Radiochemistry Facility for assistance with radiotracer synthesis.

References

[1] Stuart D, Aardalen K, Venetsanakos E, Nagel T, Wallroth M, Batt D, Ramurthy S, Poon D, Faure M, Lorenzana E, et al. (2008). RAF265 is a potent Raf kinase inhibitor with selective anti-proliferative activity *in vitro* and *in vivo*. *AACR Meeting Abstracts* **2008**, 4876.

[2] Dhomen N and Marais R (2009). BRAF signaling and targeted therapies in melanoma. *Hematol Oncol Clin North Am* **23**, 529–545.

[3] Gambhir SS, Czernin J, Schwimmer J, Silverman DH, Coleman RE, and Phelps ME (2001). A tabulated summary of the FDG PET literature. *J Nucl Med* **42**, 1S–93S.

[4] Cherry SR, Shao Y, Silverman RW, Meadors K, Young J, Jones WF, Newport D, Mooyers C, Mumcuoglu EU, Chatziioannou A, et al. (1997). MicroPET: a high resolution PET scanner for imaging small animals. *IEEE Trans Nucl Sci* **44**, 1161–1166.

[5] Pomper MG (2002). Can small animal imaging accelerate drug development? *J Cell Biochem Suppl* **39**, 211–220.

[6] Maclean D, Northrop JP, Padgett HC, and Walsh JC (2003). Drugs and probes: the symbiotic relationship between pharmaceutical discovery and imaging science. *Mol Imaging Biol* **5**, 304–311.

[7] Aboagye EO (2005). Positron emission tomography imaging of small animals in anticancer drug development. *Mol Imaging Biol* **7**, 53–58.

[8] Hargreaves RJ (2008). The role of molecular imaging in drug discovery and development. *Clin Pharmacol Ther* **83**, 349–353.

[9] Willmann JK, van Bruggen N, Dinkelborg LM, and Gambhir SS (2008). Molecular imaging in drug development. *Nat Rev Drug Discov* **7**, 591–607.

[10] Oyama N, Kim J, Jones LA, Mercer NM, Engelbach JA, Sharp TL, and Welch MJ (2002). MicroPET assessment of androgenic control of glucose and acetate uptake in the rat prostate and a prostate cancer tumor model. *Nucl Med Biol* **29**, 783–790.

[11] Cullinane C, Dorow DS, Kansara M, Conus N, Binns D, Hicks RJ, Ashman LK, McArthur GA, and Thomas DM (2005). An *in vivo* tumor model exploiting metabolic response as a biomarker for targeted drug development. *Cancer Res* **65**, 9633–9636.

[12] Jadvar H, Xiankui L, Shahinian A, Park R, Tohme M, Pinski J, and Conti PS (2005). Glucose metabolism of human prostate cancer mouse xenografts. *Mol Imaging* **4**, 91–97.

[13] Tseng JR, Kang KW, Dandekar M, Yaghoubi S, Lee JH, Christensen JG, Muir S, Vincent PW, Michaud NR, and Gambhir SS (2008). Preclinical efficacy of the c-Met inhibitor CE-355621 in a U87 MG mouse xenograft model evaluated by ^{18}F-FDG small-animal PET. *J Nucl Med* **49**, 129–134.

[14] Barthel H, Cleij MC, Collingridge DR, Hutchinson OC, Osman S, He Q, Luthra SK, Brady F, Price PM, and Aboagye EO (2003). 3′-Deoxy-3′-[^{18}F]fluorothymidine as a new marker for monitoring tumor response to antiproliferative therapy *in vivo* with positron emission tomography. *Cancer Res* **63**, 3791–3798.

[15] Sugiyama M, Sakahara H, Sato K, Harada N, Fukumoto D, Kakiuchi T, Hirano T, Kohno E, and Tsukada H (2004). Evaluation of 3′-deoxy-3′-^{18}F-fluorothymidine for monitoring tumor response to radiotherapy and photodynamic therapy in mice. *J Nucl Med* **45**, 1754–1758.

[16] Waldherr C, Mellinghoff IK, Tran C, Halpern BS, Rozengurt N, Safaei A, Weber WA, Stout D, Satyamurthy N, Barrio J, et al. (2005). Monitoring antiproliferative responses to kinase inhibitor therapy in mice with 3′-deoxy-3′-^{18}F-fluorothymidine PET. *J Nucl Med* **46**, 114–120.

[17] Leyton J, Latigo JR, Perumal M, Dhaliwal H, He Q, and Aboagye EO (2005). Early detection of tumor response to chemotherapy by 3′-deoxy-3′-[^{18}F]fluorothymidine positron emission tomography: the effect of cisplatin on a fibrosarcoma tumor model *in vivo*. *Cancer Res* **65**, 4202–4210.

[18] Tseng JR, Dandekar M, Subbarayan M, Cheng Z, Park JM, Louie S, and Gambhir SS (2005). Reproducibility of 3′-deoxy-3′-(18)F-fluorothymidine microPET studies in tumor xenografts in mice. *J Nucl Med* **46**, 1851–1857.

[19] Dandekar M, Tseng JR, and Gambhir SS (2007). Reproducibility of 2′-deoxy-2′-^{18}F fluoro-D-glucose microPET studies in mouse tumor xenografts. *J Nuc Med* **48**, 602–607.

[20] Sotiriou C and Piccart MJ (2007). Taking gene-expression profiling to the clinic: when will molecular signatures become relevant to patient care? *Nat Rev Cancer* **7**, 545–553.

[21] Fehrmann RS, Li XY, van der Zee AG, de Jong S, Te Meerman GJ, de Vries EG, and Crijns AP (2007). Profiling studies in ovarian cancer: a review. *Oncologist* **12**, 960–966.

[22] Strauss LG, Dimitrakopoulou-Strauss A, Koczan D, Koczan D, Bernd L, Haberkorn U, Ewerbeck V, and Thiesen HJ (2004). ^{18}F-FDG kinetics and gene expression in giant cell tumors. *J Nucl Med* **45**, 1528–1535.

[23] Lee JD, Yun M, Lee JM, Choi Y, Choi YH, Kim JS, Kim SJ, Kim KS, Yang WI, Park YN, et al. (2004). Analysis of gene expression profiles of hepatocellular carcinomas with regard to ^{18}F-fluorodeoxyglucose uptake pattern on positron emission tomography. *Eur J Nucl Med Mol Imaging* **31**, 1621–1630.

[24] Grigsby PW, Watson M, Powell MA, Zhang Z, and Rader JS (2006). Gene expression patterns in advanced human cervical cancer. *Int J Gynecol Cancer* **16**, 562–567.

[25] Strauss LG, Pan L, Koczan D, Klippel S, Mikolajczyk K, Burger C, Haberkorn U, Schönleben K, Thiesen HJ, and Dimitrakopoulou-Strauss A (2007). Fusion of positron emission tomography (PET) and gene array data: a new approach for the correlative analysis of molecular biological and clinical data. *IEEE Trans Med Imaging* **26**, 804–812.

[26] Erdem NF, Carlson ER, and Gerard DA (2008). Characterization of gene expression profiles of 3 different human oral squamous cell carcinoma cell lines with different invasion and metastatic capacities. *J Oral Maxillofac Surg* **66**, 918–927.

[27] von Forstner C, Egberts JH, Ammerpohl O, Niedzielska D, Buchert R, Mikecz P, Schumacher U, Peldschus K, Adam G, Pilarsky C, et al. (2008). Gene expression patterns and tumor uptake of ^{18}F-FDG, ^{18}F-FLT, and ^{18}F-FEC in PET/MRI of an orthotopic mouse xenotransplantation model of pancreatic cancer. *J Nucl Med* **49**, 1362–1370.

[28] Mootha VK, Lindgren CM, Eriksson KF, Subramanian A, Sihag S, Lehar J, Puigserver P, Carlsson E, Ridderstråle M, Laurila E, et al. (2003). PGC-1α–responsive genes involved in oxidative phosphorylation are coordinately downregulated in human diabetes. *Nat Genet* **34**, 267–273.

[29] Subramanian A, Tamayo P, Mootha VK, Mukherjee S, Ebert BL, Gillette MA, Paulovich A, Pomeroy SL, Golub TR, Lander ES, et al. (2005). Gene set enrichment analysis: a knowledge-based approach for interpreting genome-wide expression profiles. *Proc Natl Acad Sci USA* **102**, 15545–15550.

[30] Szustakowski JD, Lee J-H, Marrese CA, Kosinski PA, Nirmala NR, and Kemp DM (2006). Identification of novel pathway regulation during myogenic differentiation. *Genomics* **87**, 129–138.

[31] Storey JD and Tibshirani R (2003). Statistical significance for genomewide studies. *Proc Natl Acad Sci USA* **100**, 9440–9445.

[32] Hoffman EJ, Huang SC, and Phelps ME (1979). Quantitation in positron emission computed tomography: 1. Effect of object size. *J Comput Assist Tomogr* **3**, 299–308.

[33] Loening AM and Gambhir SS (2003). AMIDE: a free software tool for multimodality medical image analysis. *Mol Imaging* **2**, 131–137.

[34] Stuart D, Kimberly A, Lorenzana EG, Salangsang FD, Venetsanakos E, Tan N, Zhang W, Garrett E, Jallal B, and Mendel DB (2006). Characterization of a novel Raf kinase inhibitor that causes target dependent tumor regression in human melanoma xenografts expressing mutant B-Raf. *AACR Meeting Abstracts* **2006**, 4856.

[35] Kelloff GJ, Hoffman JM, Johnson B, Scher HI, Siegel BA, Cheng EY, Cheson BD, O'shaughnessy J, Guyton KZ, Mankoff DA, et al. (2005). Progress and promise of FDG-PET imaging for cancer patient management and oncologic drug development. *Clin Cancer Res* **11**, 2785–2808.

[36] Avril NE and Weber WA (2005). Monitoring response to treatment in patients utilizing PET. *Radiol Clin North Am* **43**, 189–204.

[37] Wahl RL, Hutchins GD, Buchsbaum DJ, Liebert M, Grossman HB, and Fisher S (1991). ^{18}F-2-deoxy-2-fluoro-D-glucose uptake into human tumor xenografts. Feasibility studies for cancer imaging with positron-emission tomography. *Cancer* **67**, 1544–1550.

[38] Millward MJ, Joshua A, Kefford R, Aamdal S, Thomson D, Hersey P, Toner G, and Lynch K (2005). Multi-centre phase II trial of the polyamine synthesis inhibitor SAM486A (CGP48664) in patients with metastatic melanoma. *Invest New Drugs* **23**, 253–256.

[39] Flaherty KT, Puzanov I, Kim KB, Ribas A, McArthur GA, Sosman JA, O'Dwyer PJ, Lee RJ, Grippo JF, Nolop K, et al. (2010). Inhibition of mutated, activated BRAF in metastatic melanoma. *N Engl J Med* **363**, 809–819.

[40] Parulekar WR and Eisenhauer EA (2004). Phase I trial design for solid tumor studies of targeted, non-cytotoxic agents: theory and practice. *J Natl Cancer Inst* **96**, 990–997.

[41] Reinhardt MJ, Herkel C, Altehoefer C, Finke J, and Moser E (2005). Computed tomography and ^{18}F-FDG positron emission tomography for therapy control of Hodgkin's and non–Hodgkin's lymphoma patients: when do we really need FDG-PET? *Ann Oncol* **16**, 1524–1529.

[42] Koh DM and Collins DJ (2007). Diffusion-weighted MRI in the body: applications and challenges in oncology. *AJR Am J Roentgenol* **188**, 1622–1635.

[43] Gambhir SS (2002). Molecular imaging of cancer with positron emission tomography. *Nat Rev Cancer* **2**, 683–693.

[44] Kelloff GJ, Krohn KA, Larson SM, Weissleder R, Mankoff DA, Hoffman JM, Link JM, Guyton KZ, Eckelman WC, Scher HI, et al. (2005). The progress and promise of molecular imaging probes in oncologic drug development. *Clin Cancer Res* **11**, 7967–7985.

[45] Segal E, Sirlin CB, Ooi C, Adler AS, Gollub J, Chen X, Chan BK, Matcuk GR, Barry CT, Chang HY, et al. (2007). Decoding global gene expression programs in liver cancer by noninvasive imaging. *Nat Biotechnol* **25**, 675–680.

Table W1. GSEA Data for A375M Mouse Xenograft Tumor Microarray Analysis.

Time Point	Rank within Time Point	Major Imaging Relevant Pathways	Pathway Name	Pathway Data Source	PAT Pathway ID	No. Probe Sets in Pathway	No. Probe Sets Analyzed	*P*	*q*	Effect of RAF265 on Pathway
1. Day 1: 8 h	32	Thymidine	Pyrimidine metabolism — Reference pathway	KEGG Pathways	5445010	129	83	1.17*e* − 12	8.07*e* − 11	Downregulated by RAF265
1. Day 1: 8 h	69	Glucose	Carbohydrates metabolism	MetaCore Pathway Maps	5451804	403	264	3.11*e* − 08	1.09*e* − 06	Downregulated by RAF265
1. Day 1: 8 h	75	Thymidine	Nucleotide metabolism	MetaCore Pathway Maps	5451807	367	224	2.45*e* − 07	7.46*e* − 06	Downregulated by RAF265
1. Day 1: 8 h	268	Apoptosis	Apoptosis and survival	MetaCore Pathway Maps	5451812	488	242	8.46*e* − 04	7.05*e* − 03	Downregulated by RAF265
1. Day 1: 8 h	305	Thymidine	Nucleotide kinase	PANTHER Library and Pathways	5482627	82	49	1.56*e* − 03	1.16*e* − 02	Downregulated by RAF265
1. Day 1: 8 h	353	Apoptosis	Apoptosis and survival_Apoptotic TNF family pathways	MetaCore Pathway Maps	5452156	79	39	2.73*e* − 03	1.77*e* − 02	Downregulated by RAF265
1. Day 1: 8 h	361	Apoptosis	Apoptosis and survival_DNA damages-induced apoptosis	MetaCore Pathway Maps	5452080	27	14	2.92*e* − 03	1.86*e* − 02	Downregulated by RAF265
1. Day 1: 8 h	516	Thymidine	Pyrimidine metabolism	PANTHER Library and Pathways	5482931	62	38	1.04*e* − 02	4.82*e* − 02	Downregulated by RAF265
1. Day 1: 8 h	525	Apoptosis	Apoptosis_Apoptotic mitochondria	MetaCore GeneGo Processes	5451700	171	85	1.10*e* − 02	5.02*e* − 02	Downregulated by RAF265
1. Day 1: 8 h	596	Apoptosis	Apoptosis — *Homo sapiens* (human)	KEGG Pathways	5445469	156	83	1.62*e* − 02	6.54*e* − 02	Downregulated by RAF265
1. Day 1: 8 h	597	Apoptosis	Apoptosis — Reference pathway	KEGG Pathways	5446108	156	83	1.62*e* − 02	6.54*e* − 02	Downregulated by RAF265
1. Day 1: 8 h	628	EGFR	Development_EGF signaling pathway	MetaCore Pathway Maps	5451866	65	31	1.86*e* − 02	7.13*e* − 02	Downregulated by RAF265
1. Day 1: 8 h	782	Glucose	Amino sugars metabolism — *Homo sapiens* (human)	KEGG Pathways	5445406	37	28	3.19*e* − 02	1.01*e* − 01	Downregulated by RAF265
1. Day 1: 8 h	783	Glucose	Amino sugars metabolism — Reference pathway	KEGG Pathways	5445046	37	28	3.19*e* − 02	1.01*e* − 01	Downregulated by RAF265
1. Day 1: 8 h	1089	Glucose	Sugar transporter	PANTHER Library and Pathways	5463809	44	30	8.10*e* − 02	1.84*e* − 01	Upregulated by RAF265
1. Day 1: 8 h	1124	Apoptosis	Apoptosis	PANTHER Library and Pathways	5482864	810	457	8.60*e* − 02	1.91*e* − 01	Downregulated by RAF265
1. Day 1: 8 h	1135	EGFR	Development_ERBB family signaling	MetaCore Pathway Maps	5451993	46	24	8.92*e* − 02	1.96*e* − 01	Downregulated by RAF265
1. Day 1: 8 h	1430	Glucose	Glycolysis and gluconeogenesis (short map)	MetaCore Pathway Maps	5452216	49	33	1.53*e* − 01	2.72*e* − 01	Downregulated by RAF265
1. Day 1: 8 h	1546	Glucose	Glycolysis/Gluconeogenesis — Reference pathway	KEGG Pathways	5444988	94	63	1.80*e* − 01	2.98*e* − 01	Downregulated by RAF265
1. Day 1: 8 h	1547	Glucose	Glycolysis/Gluconeogenesis — *Homo sapiens* (human)	KEGG Pathways	5445353	94	63	1.80*e* − 01	2.98*e* − 01	Downregulated by RAF265
1. Day 1: 8 h	1565	Apoptosis	Apoptosis signaling pathway	PANTHER Library and Pathways	5483119	242	120	1.84*e* − 01	3.02*e* − 01	Downregulated by RAF265
1. Day 1: 8 h	1857	EGFR	ErbB signaling pathway — *Homo sapiens* (human)	KEGG Pathways	5446835	167	84	2.53*e* − 01	3.52*e* − 01	Downregulated by RAF265
1. Day 1: 8 h	1858	EGFR	ErbB signaling pathway — Reference pathway	KEGG Pathways	5446843	167	84	2.53*e* − 01	3.52*e* − 01	Downregulated by RAF265
1. Day 1: 8 h	2120	Glucose	Hexokinase	PANTHER Library and Pathways	5462148	7	5	3.28*e* − 01	4.03*e* − 01	Downregulated by RAF265
1. Day 1: 8 h	2121	Glucose	Hexokinase	PANTHER Library and Pathways	5484985	7	5	3.28*e* − 01	4.03*e* − 01	Downregulated by RAF265
1. Day 1: 8 h	2122	Glucose	Hexokinase	PANTHER Library and Pathways	5483869	7	5	3.28*e* − 01	4.03*e* − 01	Downregulated by RAF265
1. Day 1: 8 h	2123	Glucose	Hexokinase	PANTHER Library and Pathways	5483870	7	5	3.28*e* − 01	4.03*e* − 01	Downregulated by RAF265
1. Day 1: 8 h	2318	EGFR	Development_EGFR signaling through small GTPases	MetaCore Pathway Maps	5452062	41	22	3.96*e* − 01	4.46*e* − 01	Downregulated by RAF265
1. Day 1: 8 h	2322	Glucose	Glycolysis and gluconeogenesis p. 1	MetaCore Pathway Maps	5451914	24	19	3.96*e* − 01	4.46*e* − 01	Downregulated by RAF265
1. Day 1: 8 h	2510	EGFR	EGF receptor signaling pathway	PANTHER Library and Pathways	5483165	264	134	4.59*e* − 01	4.80*e* − 01	Downregulated by RAF265
1. Day 1: 8 h	2599	EGFR	Development_EGFR signaling through PIP3	MetaCore Pathway Maps	5451970	32	13	4.92*e* − 01	4.96*e* − 01	Upregulated by RAF265
1. Day 1: 8 h	2869	Glucose	Glycogen metabolism	MetaCore Pathway Maps	5452161	15	15	5.80*e* − 01	5.32*e* − 01	Downregulated by RAF265
1. Day 1: 8 h	2972	Glucose	Carbohydrate kinase	PANTHER Library and Pathways	5482771	39	26	6.11*e* − 01	5.43*e* − 01	Downregulated by RAF265
1. Day 1: 8 h	3629	Glucose	Carbohydrate transporter	PANTHER Library and Pathways	5482755	44	28	8.60*e* − 01	6.30*e* − 01	Upregulated by RAF265
2. Day 1: 24 h	45	Glucose	Carbohydrates metabolism	MetaCore Pathway Maps	5451804	403	264	5.05*e* − 09	2.07*e* − 07	Downregulated by RAF265
2. Day 1: 24 h	61	Thymidine	Pyrimidine metabolism — Reference pathway	KEGG Pathways	5445010	129	83	2.69*e* − 08	8.38*e* − 07	Downregulated by RAF265
2. Day 1: 24 h	76	Apoptosis	Apoptosis and survival	MetaCore Pathway Maps	5451812	488	242	1.20*e* − 07	3.10*e* − 06	Downregulated by RAF265
2. Day 1: 24 h	103	Apoptosis	Apoptosis — *Homo sapiens* (human)	KEGG Pathways	5445469	156	83	7.46*e* − 07	1.42*e* − 05	Downregulated by RAF265
2. Day 1: 24 h	104	Apoptosis	Apoptosis — Reference pathway	KEGG Pathways	5446108	156	83	7.46*e* − 07	1.42*e* − 05	Downregulated by RAF265
2. Day 1: 24 h	133	Apoptosis	Apoptosis and survival_DNA damages-induced apoptosis	MetaCore Pathway Maps	5452080	27	14	3.25*e* − 06	4.86*e* − 05	Downregulated by RAF265
2. Day 1: 24 h	136	Glucose	Glycolysis and gluconeogenesis (short map)	MetaCore Pathway Maps	5452216	49	33	4.16*e* − 06	6.08*e* − 05	Downregulated by RAF265
2. Day 1: 24 h	266	Glucose	Glycolysis/Gluconeogenesis — Reference pathway	KEGG Pathways	5444988	94	63	4.07*e* − 04	2.89*e* − 03	Downregulated by RAF265
2. Day 1: 24 h	267	Glucose	Glycolysis/Gluconeogenesis — *Homo sapiens* (human)	KEGG Pathways	5445353	94	63	4.07*e* − 04	2.89*e* − 03	Downregulated by RAF265
2. Day 1: 24 h	438	EGFR	Development_EGF signaling pathway	MetaCore Pathway Maps	5451866	65	31	3.49*e* − 03	1.53*e* − 02	Downregulated by RAF265
2. Day 1: 24 h	480	Apoptosis	Apoptosis signaling pathway	PANTHER Library and Pathways	5483119	242	120	4.74*e* − 03	1.91*e* − 02	Downregulated by RAF265
2. Day 1: 24 h	654	Glucose	Carbohydrate kinase	PANTHER Library and Pathways	5482771	39	26	1.32*e* − 02	3.96*e* − 02	Downregulated by RAF265
2. Day 1: 24 h	697	Thymidine	Nucleotide metabolism	MetaCore Pathway Maps	5451807	367	224	1.56*e* − 02	4.42*e* − 02	Downregulated by RAF265
2. Day 1: 24 h	703	EGFR	Development_ERBB family signaling	MetaCore Pathway Maps	5451993	46	24	1.58*e* − 02	4.45*e* − 02	Downregulated by RAF265
2. Day 1: 24 h	816	Glucose	SUGAR TRANSPORTER	PANTHER Library and Pathways	5463809	44	30	2.38*e* − 02	5.86*e* − 02	Upregulated by RAF265
2. Day 1: 24 h	900	Apoptosis	Apoptosis_Apoptotic mitochondria	MetaCore GeneGo Processes	5451700	171	85	3.36*e* − 02	7.58*e* − 02	Downregulated by RAF265
2. Day 1: 24 h	939	Glucose	Amino sugars metabolism — *Homo sapiens* (human)	KEGG Pathways	5445406	37	28	3.77*e* − 02	8.10*e* − 02	Downregulated by RAF265
2. Day 1: 24 h	940	Glucose	Amino sugars metabolism — Reference pathway	KEGG Pathways	5445046	37	28	3.77*e* − 02	8.10*e* − 02	Downregulated by RAF265
2. Day 1: 24 h	1039	Apoptosis	Apoptosis and survival_Apoptotic TNF family pathways	MetaCore Pathway Maps	5452156	79	39	4.80*e* − 02	9.44*e* − 02	Downregulated by RAF265

Table W1. (*continued*)

Time Point	Rank within Time Point	Major Imaging Relevant Pathways	Pathway Name	Pathway Data Source	PAT Pathway ID	No. Probe Sets in Pathway	No. Probe Sets Analyzed	*P*	*q*	Effect of RAF265 on Pathway
2. Day 1: 24 h	1069	EGFR	ErbB signaling pathway — *Homo sapiens* (human)	KEGG Pathways	5446835	167	84	5.36*e* – 02	1.02*e* – 01	Downregulated by RAF265
2. Day 1: 24 h	1070	EGFR	ErbB signaling pathway — Reference pathway	KEGG Pathways	5446843	167	84	5.36*e* – 02	1.02*e* – 01	Downregulated by RAF265
2. Day 1: 24 h	1110	Glucose	Glycogen metabolism	MetaCore Pathway Maps	5452161	15	15	5.97*e* – 02	1.10*e* – 01	Downregulated by RAF265
2. Day 1: 24 h	1558	EGFR	Development_EGFR signaling through small GTPases	MetaCore Pathway Maps	5452062	41	22	1.39*e* – 01	1.87*e* – 01	Downregulated by RAF265
2. Day 1: 24 h	1635	Thymidine	Nucleotide kinase	PANTHER Library and Pathways	5482627	82	49	1.53*e* – 01	1.97*e* – 01	Downregulated by RAF265
2. Day 1: 24 h	1668	Thymidine	Pyrimidine metabolism	PANTHER Library and Pathways	5482931	62	39	1.62*e* – 01	2.04*e* – 01	Downregulated by RAF265
2. Day 1: 24 h	1984	EGFR	EGF receptor signaling pathway	PANTHER Library and Pathways	5483165	264	134	2.34*e* – 01	2.51*e* – 01	Downregulated by RAF265
2. Day 1: 24 h	2234	Apoptosis	Apoptosis	PANTHER Library and Pathways	5482864	810	457	3.04*e* – 01	2.92*e* – 01	Downregulated by RAF265
2. Day 1: 24 h	2486	Glucose	Hexokinase	PANTHER Library and Pathways	5483869	7	5	3.90*e* – 01	3.39*e* – 01	Downregulated by RAF265
2. Day 1 24 h	2487	Glucose	Hexokinase	PANTHER Library and Pathways	5483870	7	5	3.90*e* – 01	3.39*e* – 01	Downregulated by RAF265
2. Day 1 24 h	2488	Glucose	Hexokinase	PANTHER Library and Pathways	5484985	7	5	3.90*e* – 01	3.39*e* – 01	Downregulated by RAF265
2. Day 1 24 h	2489	Glucose	Hexokinase	PANTHER Library and Pathways	5462148	7	5	3.90*e* – 01	3.39*e* – 01	Downregulated by RAF265
2. Day 1: 24 h	2708	Glucose	Carbohydrate transporter	PANTHER Library and Pathways	5482755	44	28	4.63*e* – 01	3.71*e* – 01	Upregulated by RAF265
2. Day 1: 24 h	2936	Glucose	Glycolysis and gluconeogenesis p. 1	MetaCore Pathway Maps	5451914	24	19	5.50*e* – 01	4.08*e* – 01	Downregulated by RAF265
2. Day 1: 24 h	3159	EGFR	Development_EGFR signaling through PIP3	MetaCore Pathway Maps	5451970	32	13	6.43*e* – 01	4.45*e* – 01	Upregulated by RAF265
3. Day 8	35	Thymidine	Pyrimidine metabolism — Reference pathway	KEGG Pathways	5445010	129	83	7.11*e* – 15	3.74*e* – 13	Downregulated by RAF265
3. Day 8	66	Thymidine	Nucleotide metabolism	MetaCore Pathway Maps	5451807	367	224	4.15*e* – 11	1.25*e* – 09	Downregulated by RAF265
3. Day 8	122	Glucose	Glycolysis and gluconeogenesis (short map)	MetaCore Pathway Maps	5452216	49	33	8.63*e* – 08	1.40*e* – 06	Downregulated by RAF265
3. Day 8	132	Glucose	Carbohydrates metabolism	MetaCore Pathway Maps	5451804	403	264	2.14*e* – 07	3.23*e* – 06	Downregulated by RAF265
3. Day 8	141	Apoptosis	Apoptosis_Apoptotic mitochondria	MetaCore GeneGo Processes	5451700	171	85	3.44*e* – 07	4.88*e* – 06	Downregulated by RAF265
3. Day 8	163	Apoptosis	Apoptosis and survival	MetaCore Pathway Maps	5451812	488	242	1.06*e* – 06	1.28*e* – 05	Downregulated by RAF265
3. Day 8	204	Glucose	Carbohydrate kinase	PANTHER Library and Pathways	5482771	39	26	7.48*e* – 06	7.29*e* – 05	Downregulated by RAF265
3. Day 8	219	Apoptosis	Apoptosis signaling pathway	PANTHER Library and Pathways	5483119	242	120	1.05*e* – 05	9.58*e* – 05	Downregulated by RAF265
3. Day 8	225	Glucose	Glycolysis/Gluconeogenesis — *Homo sapiens* (human)	KEGG Pathways	5445353	94	63	1.63*e* – 05	1.43*e* – 04	Downregulated by RAF265
3. Day 8	226	Glucose	Glycolysis/Gluconeogenesis — Reference pathway	KEGG Pathways	5444988	94	63	1.63*e* – 05	1.43*e* – 04	Downregulated by RAF265
3. Day 8	227	Apoptosis	Apoptosis — *Homo sapiens* (human)	KEGG Pathways	5445469	156	83	1.73*e* – 05	1.50*e* – 04	Downregulated by RAF265
3. Day 8	228	Apoptosis	Apoptosis — Reference pathway	KEGG Pathways	5446108	156	83	1.73*e* – 05	1.50*e* – 04	Downregulated by RAF265
3. Day 8	320	Glucose	Amino sugars metabolism — *Homo sapiens* (human)	KEGG Pathways	5445406	37	28	1.87*e* – 04	1.13*e* – 03	Downregulated by RAF265
3. Day 8	321	Glucose	Amino sugars metabolism — Reference pathway	KEGG Pathways	5445046	37	28	1.87*e* – 04	1.13*e* – 03	Downregulated by RAF265
3. Day 8	406	Thymidine	Pyrimidine metabolism	PANTHER Library and Pathways	5482931	62	38	8.99*e* – 04	4.23*e* – 03	Downregulated by RAF265
3. Day 8	459	Glucose	Glycolysis and gluconeogenesis p. 1	MetaCore Pathway Maps	5451914	24	19	1.61*e* – 03	6.80*e* – 03	Downregulated by RAF265
3. Day 8	709	Apoptosis	Apoptosis and survival_Apoptotic TNF family pathways	MetaCore Pathway Maps	5452156	79	39	1.28*e* – 02	3.54*e* – 02	Downregulated by RAF265
3. Day 8	1002	Glucose	Glycogen metabolism	MetaCore Pathway Maps	5452161	15	15	3.78*e* – 02	7.63*e* – 02	Downregulated by RAF265
3. Day 8	1276	EGFR	Development_EGF signaling pathway	MetaCore Pathway Maps	5451866	65	31	7.29*e* – 02	1.18*e* – 01	Downregulated by RAF265
3. Day 8	1325	Thymidine	Nucleotide kinase	PANTHER Library and Pathways	5482627	82	49	7.87*e* – 02	1.23*e* – 01	Downregulated by RAF265
3. Day 8	1641	Apoptosis	Apoptosis and survival_DNA damages-induced apoptosis	MetaCore Pathway Maps	5452080	27	14	1.43*e* – 01	1.82*e* – 01	Downregulated by RAF265
3. Day 8	1651	Glucose	Hexokinase	PANTHER Library and Pathways	5484985	7	5	1.44*e* – 01	1.83*e* – 01	Downregulated by RAF265
3. Day 8	1652	Glucose	Hexokinase	PANTHER Library and Pathways	5483869	7	5	1.44*e* – 01	1.83*e* – 01	Downregulated by RAF265
3. Day 8	1653	Glucose	Hexokinase	PANTHER Library and Pathways	5462148	7	5	1.44*e* – 01	1.83*e* – 01	Downregulated by RAF265
3. Day 8	1654	Glucose	Hexokinase	PANTHER Library and Pathways	5483870	7	5	1.44*e* – 01	1.83*e* – 01	Downregulated by RAF265
3. Day 8	1661	Apoptosis	Apoptosis	PANTHER Library and Pathways	5482864	810	456	1.45*e* – 01	1.84*e* – 01	Downregulated by RAF265
3. Day 8	2362	Glucose	Sugar transporter	PANTHER Library and Pathways	5463809	44	30	3.45*e* – 01	3.12*e* – 01	Upregulated by RAF265
3. Day 8	2929	Glucose	Carbohydrate transporter	PANTHER Library and Pathways	5482755	44	28	5.63*e* – 01	4.15*e* – 01	Upregulated by RAF265
3. Day 8	3107	EGFR	EGF receptor signaling pathway	PANTHER Library and Pathways	5483165	264	134	6.32*e* – 01	4.40*e* – 01	Downregulated by RAF265
3. Day 8	3245	EGFR	ErbB signaling pathway — *Homo sapiens* (human)	KEGG Pathways	5446835	167	84	6.86*e* – 01	4.58*e* – 01	Downregulated by RAF265
3. Day 8	3246	EGFR	ErbB signaling pathway — Reference pathway	KEGG Pathways	5446843	167	84	6.86*e* – 01	4.58*e* – 01	Downregulated by RAF265
3. Day 8	3299	EGFR	Development_EGFR signaling through PIP3	MetaCore Pathway Maps	5451970	32	13	7.13*e* – 01	4.68*e* – 01	Upregulated by RAF265
3. Day 8	3769	EGFR	Development_EGFR signaling through small GTPases	MetaCore Pathway Maps	5452062	41	22	8.92*e* – 01	5.16*e* – 01	Downregulated by RAF265
3. Day 8	3866	EGFR	Development_ERBB family signaling	MetaCore Pathway Maps	5451993	46	24	9.32*e* – 01	5.26*e* – 01	Upregulated by RAF265
4. Day 14	33	Thymidine	Pyrimidine metabolism — Reference pathway	KEGG Pathways	5445010	129	83	8.88*e* – 16	4.29*e* – 14	Downregulated by RAF265
4. Day 14	65	Thymidine	Nucleotide metabolism	MetaCore Pathway Maps	5451807	367	224	1.82*e* – 12	5.28*e* – 11	Downregulated by RAF265
4. Day 14	96	Apoptosis	Apoptosis and survival	MetaCore Pathway Maps	5451812	488	242	4.95*e* – 10	9.88*e* – 09	Downregulated by RAF265
4. Day 14	133	Glucose	Carbohydrate kinase	PANTHER Library and Pathways	5482771	39	26	2.73*e* – 08	3.95*e* – 07	Downregulated by RAF265

Table W1. (*continued*)

Time Point	Rank within Time Point	Major Imaging Relevant Pathways	Pathway Name	Pathway Data Source	PAT Pathway ID	No. Probe Sets in Pathway	No. Probe Sets Analyzed	*P*	*q*	Effect of RAF265 on Pathway
4. Day 14	151	Apoptosis	Apoptosis_Apoptotic mitochondria	MetaCore GeneGo Processes	5451700	171	85	6.23*e* − 08	8.02*e* − 07	Downregulated by RAF265
4. Day 14	156	Glucose	Carbohydrates metabolism	MetaCore Pathway Maps	5451804	403	264	7.28*e* − 08	9.07*e* − 07	Downregulated by RAF265
4. Day 14	163	Glucose	Glycolysis and gluconeogenesis (short map)	MetaCore Pathway Maps	5452216	49	33	1.31*e* − 07	1.55*e* − 06	Downregulated by RAF265
4. Day 14	207	Apoptosis	Apoptosis and survival_Apoptotic TNF family pathways	MetaCore Pathway Maps	5452156	79	39	1.23*e* − 06	1.13*e* − 05	Downregulated by RAF265
4. Day 14	211	Apoptosis	Apoptosis signaling pathway	PANTHER Library and Pathways	5483119	242	120	1.59*e* − 06	1.44*e* − 05	Downregulated by RAF265
4. Day 14	220	Apoptosis	Apoptosis — Reference pathway	KEGG Pathways	5446108	156	83	2.32*e* − 06	2.01*e* − 05	Downregulated by RAF265
4. Day 14	221	Apoptosis	Apoptosis — *Homo sapiens* (human)	KEGG Pathways	5445469	156	83	2.32*e* − 06	2.01*e* − 05	Downregulated by RAF265
4. Day 14	332	Glucose	Glycolysis/Gluconeogenesis — Reference pathway	KEGG Pathways	5444988	94	63	1.06*e* − 04	5.89*e* − 04	Downregulated by RAF265
4. Day 14	333	Glucose	Glycolysis/Gluconeogenesis — *Homo sapiens* (human)	KEGG Pathways	5445353	94	63	1.06*e* − 04	5.89*e* − 04	Downregulated by RAF265
4. Day 14	476	Glucose	Glycolysis and gluconeogenesis p. 1	MetaCore Pathway Maps	5451914	24	19	1.33*e* − 03	5.11*e* − 03	Downregulated by RAF265
4. Day 14	578	Glucose	Amino sugars metabolism — Reference pathway	KEGG Pathways	5445046	37	28	3.08*e* − 03	9.80*e* − 03	Downregulated by RAF265
4. Day 14	579	Glucose	Amino sugars metabolism — *Homo sapiens* (human)	KEGG Pathways	5445406	37	28	3.08*e* − 03	9.80*e* − 03	Downregulated by RAF265
4. Day 14	829	Glucose	Glycogen metabolism	MetaCore Pathway Maps	5452161	15	15	1.26*e* − 02	2.86*e* − 02	Downregulated by RAF265
4. Day 14	839	EGFR	Development_EGF signaling pathway	MetaCore Pathway Maps	5451866	65	31	1.30*e* − 02	2.93*e* − 02	Downregulated by RAF265
4. Day 14	844	Thymidine	Pyrimidine metabolism	PANTHER Library and Pathways	5482931	62	38	1.32*e* − 02	2.97*e* − 02	Downregulated by RAF265
4. Day 14	992	Glucose	Hexokinase	PANTHER Library and Pathways	5484985	7	5	2.35*e* − 02	4.51*e* − 02	Downregulated by RAF265
4. Day 14	993	Glucose	Hexokinase	PANTHER Library and Pathways	5483869	7	5	2.35*e* − 02	4.51*e* − 02	Downregulated by RAF265
4. Day 14	994	Glucose	HEXOKINASE	PANTHER Library and Pathways	5462148	7	5	2.35*e* − 02	4.51*e* − 02	Downregulated by RAF265
4. Day 14	995	Glucose	Hexokinase	PANTHER Library and Pathways	5483870	7	5	2.35*e* − 02	4.51*e* − 02	Downregulated by RAF265
4. Day 14	1087	Apoptosis	Apoptosis	PANTHER Library and Pathways	5482864	810	457	3.34*e* − 02	5.86*e* − 02	Downregulated by RAF265
4. Day 14	1255	EGFR	Development_ERBB family signaling	MetaCore Pathway Maps	5451993	46	24	5.32*e* − 02	8.14*e* − 02	Downregulated by RAF265
4. Day 14	1270	Thymidine	Nucleotide kinase	PANTHER Library and Pathways	5482627	82	48	5.58*e* − 02	8.44*e* − 02	Downregulated by RAF265
4. Day 14	1423	Glucose	Sugar transporter	PANTHER Library and Pathways	5463809	44	30	8.07*e* − 02	1.10*e* − 01	Upregulated by RAF265
4. Day 14	1501	EGFR	Development_EGFR signaling through PIP3	MetaCore Pathway Maps	5451970	32	13	9.48*e* − 02	1.22*e* − 01	Downregulated by RAF265
4. Day 14	1535	EGFR	Development_EGFR signaling through small GTPases	MetaCore Pathway Maps	5452062	41	22	1.01*e* − 01	1.28*e* − 01	Downregulated by RAF265
4. Day 14	1577	EGFR	EGF receptor signaling pathway	PANTHER Library and Pathways	5483165	264	134	1.11*e* − 01	1.36*e* − 01	Downregulated by RAF265
4. Day 14	1816	Apoptosis	Apoptosis and survival_DNA damages-induced apoptosis	MetaCore Pathway Maps	5452080	27	14	1.63*e* − 01	1.74*e* − 01	Downregulated by RAF265
4. Day 14	2444	Glucose	Carbohydrate transporter	PANTHER Library and Pathways	5482755	44	28	3.42*e* − 01	2.78*e* − 01	Upregulated by RAF265
4. Day 14	2977	EGFR	ErbB signaling pathway — *Homo sapiens* (human)	KEGG Pathways	5446835	167	84	5.41*e* − 01	3.62*e* − 01	Downregulated by RAF265
4. Day 14	2978	EGFR	ErbB signaling pathway — Reference pathway	KEGG Pathways	5446843	167	84	5.41*e* − 01	3.62*e* − 01	Downregulated by RAF265

The *P* and *q* values (columns 9 and 10) for 34 pathways across all time points (selected as described in Materials and Methods) are listed. The time at which the xenografts were harvested (column 1), rank of pathway by *q* value compared with all 4014 pathways interrogated by GSEA (column 2), relevant imaging modality (column 3), pathway name (column 4), pathway data source (column 5), no. probe sets analyzed (column 8), and effect of RAF265 on the pathway (column 11) are also indicated.

Figure W1. Rotating three-dimensional volume rendering of a small animal FDG PET image of a typical nude mouse with an A375M tumor xenograft in the right upper flank. The image was obtained one hour after the injection of 200 μCi of FDG. Intense activity is seen in the right upper flank at the site of the tumor xenograft. Normal intense physiologic activity is seen in the brain, heart, bladder, and kidneys. Mild physiologic activity is seen in the liver, bowel, and muscles.

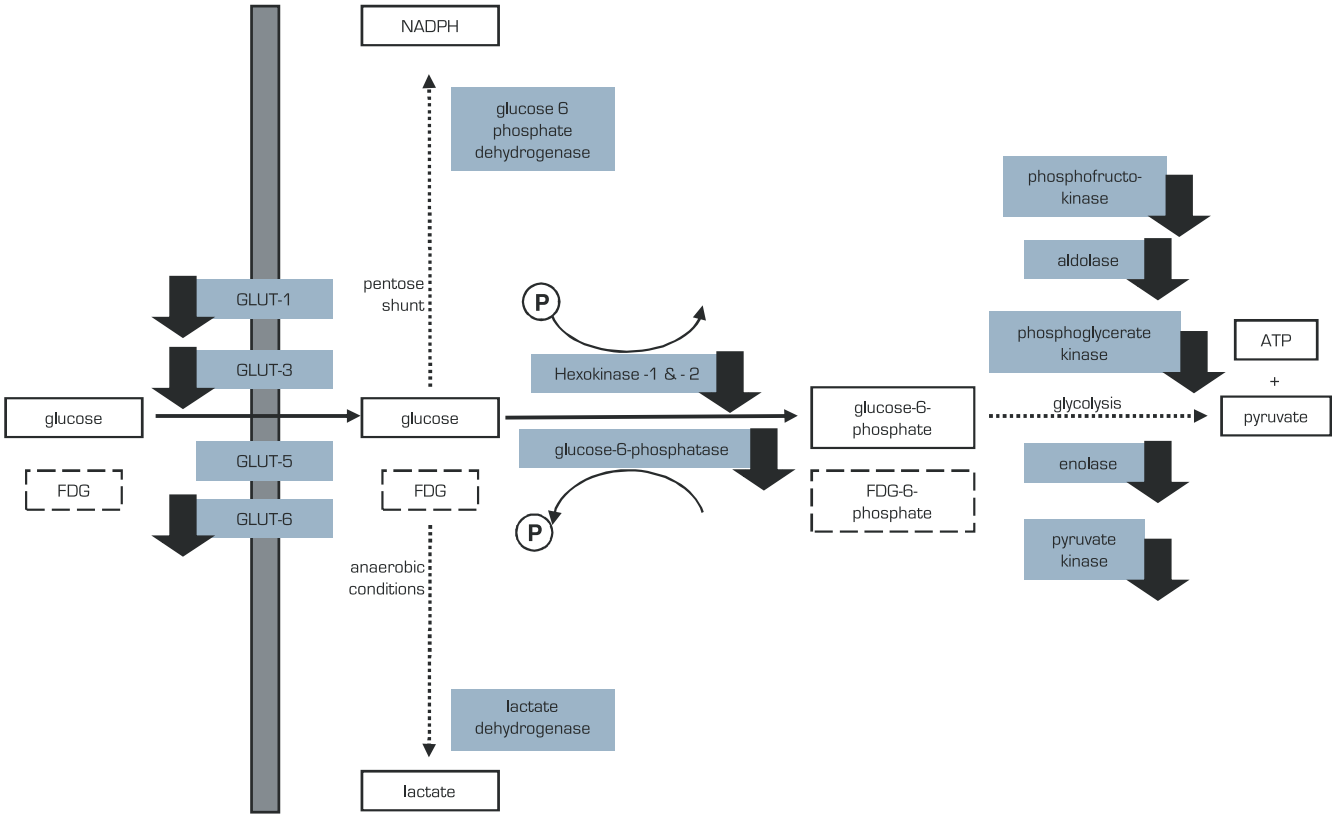

Figure W2. Regulation of glucose transport and glycolysis genes by RAF265. Genes involved in glucose transport and glycolysis (shaded rectangles), glucose metabolism substrates (open rectangles), FDG metabolism substrates (dashed rectangles), and plasma membrane (dark gray bar at the left) are indicated. Arrows indicate genes significantly downregulated in A375M xenografts after RAF265 treatment for at least one time point (DNA microarray analysis, $P < .05$ with Bonferroni correction. One probe set with the greatest dynamic range across all samples was evaluated for ALDOA, ALDOC, ENO1, ENO2, G6PC, G6PC3, G6PD, HK1, HK2, LDHA, LDHB, LDHC, PFKFB1, PFKFB2, PFKFB3, PFKFB4, PFKP, PGK1, PGK2, PKM2, SLC2A1, SLC2A3, SLC2A5, SLC2A6).